



Showcasing research from Professor Mi Hee Lim's laboratory, Department of Chemistry, Korea Advanced Institute of Science and Technology (KAIST), Daejeon, Korea.

Designing multi-target-directed flavonoids: a strategic approach to Alzheimer's disease

This work highlights a multidisciplinary strategic approach for designing multi-target-directed flavonoids as chemical reagents for Alzheimer's disease and serves as a roadmap for designing small molecules as chemical tools or therapeutic candidates in neurodegenerative disorders.

As featured in:



See Young-Ho Lee, Mi Hee Lim *et al.*, *Chem. Sci.*, 2023, **14**, 9293.

Cite this: *Chem. Sci.*, 2023, 14, 9293

All publication charges for this article have been paid for by the Royal Society of Chemistry

## Designing multi-target-directed flavonoids: a strategic approach to Alzheimer's disease†

Seongmin Park,<sup>‡a</sup> Mingeun Kim,<sup>‡a</sup> Yuxi Lin,<sup>b</sup> Mannkyu Hong,<sup>ac</sup> Geewoo Nam,<sup>a</sup> Adam Mieczkowski,<sup>d</sup> József Kardos,<sup>e</sup> Young-Ho Lee<sup>\*bfgghi</sup> and Mi Hee Lim<sup>†b</sup><sup>\*a</sup>

The underlying causes of Alzheimer's disease (AD) remain a mystery, with multiple pathological components, including oxidative stress, acetylcholinesterase, amyloid- $\beta$ , and metal ions, all playing a role. Here we report a strategic approach to designing flavonoids that can effectively tackle multiple pathological elements involved in AD. Our systematic investigations revealed key structural features for flavonoids to simultaneously target and regulate pathogenic targets. Our findings led to the development of a highly promising flavonoid that exhibits a range of functions, based on a complete structure–activity relationship analysis. Furthermore, our mechanistic studies confirmed that this flavonoid's versatile reactivities are driven by its redox potential and direct interactions with pathogenic factors. This work highlights the potential of multi-target-directed flavonoids as a novel solution in the fight against AD.

Received 10th February 2023  
Accepted 2nd August 2023

DOI: 10.1039/d3sc00752a

rsc.li/chemical-science

### Introduction

The intertwined network among multiple pathological factors, such as free radicals, acetylcholinesterase (AChE), metal-free amyloid- $\beta$  (A $\beta$ ), and metal-bound A $\beta$  (metal-A $\beta$ ) (Fig. 1a and b), has given the difficulty in combating Alzheimer's disease (AD).<sup>1–5</sup> Oxidative stress characterized by dysregulated free radicals can damage lipids, nucleic acids, and proteins, which leads to organelle dysfunction and cell death.<sup>6–8</sup> As illustrated in the cholinergic hypothesis, AChE is associated with the development of AD.<sup>3,9</sup> The synaptic concentration of the neurotransmitter acetylcholine (ACh) is adjusted by the catalytic

activity of AChE;<sup>10–12</sup> however, the abnormally reduced level of ACh can be driven by the increased amount of AChE.<sup>3,10,13</sup> In addition, highly concentrated AChE within senile plaques (SPs) can co-localize and interact with A $\beta$  species, resulting in the AChE–A $\beta$  complexation and the acceleration of amyloid aggregation.<sup>13</sup> A $\beta$  peptides tend to aggregate into toxic self-assembled aggregates, such as oligomers and fibrils.<sup>14–19</sup> In particular, metastable and structured A $\beta$  oligomers are known to trigger membrane disruption, abnormal cellular signaling, and organelle dysfunction.<sup>1,9,15</sup> High concentrations of metal ions [e.g., Cu(I/II) and Zn(II)] are also found in the SPs of AD patients, and they can affect the conformation and aggregation behaviors of A $\beta$  by their coordination to A $\beta$ .<sup>20–24</sup> Moreover, redox-active Cu(I/II)-bound A $\beta$  species can produce reactive oxygen species (ROS) via Fenton-like reactions and, consequently, aggravate oxidative stress.<sup>25–29</sup>

Several pharmacological trials employing antioxidants (e.g., vitamin E),<sup>30,31</sup> AChE inhibitors (e.g., donepezil, galantamine, rivastigmine),<sup>3,25</sup> and anti-A $\beta$  drugs (e.g., aducanumab and lecanemab)<sup>32–34</sup> have been attempted to prevent the progression of AD. Such single target-based therapeutics can temporarily relieve symptoms,<sup>3,25</sup> and their efficacies are still questionable, however.<sup>9,35</sup> Thus, significant endeavors in designing chemical reagents capable of targeting and modulating two or more pathogenic elements have been made to elucidate the complex pathology of AD and discover effective therapeutic candidates.<sup>3,9,24,29,36</sup> Herein, we illustrate a strategic approach to designing flavonoids that can target multiple pathogenic factors, including free radicals, AChE, metal-free A $\beta$ , and metal-A $\beta$ , as depicted in Fig. 1a and b, and modulate their reactivities (*vide infra*). We identified key structural features shown in flavonoids that are responsible for versatile reactivities against

<sup>a</sup>Department of Chemistry, Korea Advanced Institute of Science and Technology (KAIST), Daejeon 34141, Republic of Korea. E-mail: miheelim@kaist.ac.kr

<sup>b</sup>Research Center for Bioconvergence Analysis, Korea Basic Science Institute (KBSI), Ochang, Chungbuk 28119, Republic of Korea. E-mail: mr0505@kbsi.re.kr

<sup>c</sup>Center for Catalytic Hydrocarbon Functionalizations, Institute for Basic Science (IBS), Daejeon 34141, Republic of Korea

<sup>d</sup>Institute of Biochemistry and Biophysics, Polish Academy of Sciences, Pawińskiego 5a, 02-106 Warsaw, Poland

<sup>e</sup>ELTE NAP Neuroimmunology Research Group, Department of Biochemistry, Institute of Biology, ELTE Eötvös Loránd University, Budapest 1117, Hungary

<sup>f</sup>Bio-Analytical Science, University of Science and Technology (UST), Daejeon 34113, Republic of Korea

<sup>g</sup>Graduate School of Analytical Science and Technology, Chungnam National University, Daejeon 34134, Republic of Korea

<sup>h</sup>Department of Systems Biotechnology, Chung-Ang University (CAU), Gyeonggi 17546, Republic of Korea

<sup>i</sup>Frontier Research Institute for Interdisciplinary Sciences (FRIS), Tohoku University, Sendai, Miyagi 980-8578, Japan

† Electronic supplementary information (ESI) available: Experimental section and Fig. S1–S23. See DOI: <https://doi.org/10.1039/d3sc00752a>

‡ These authors contributed equally to this work.



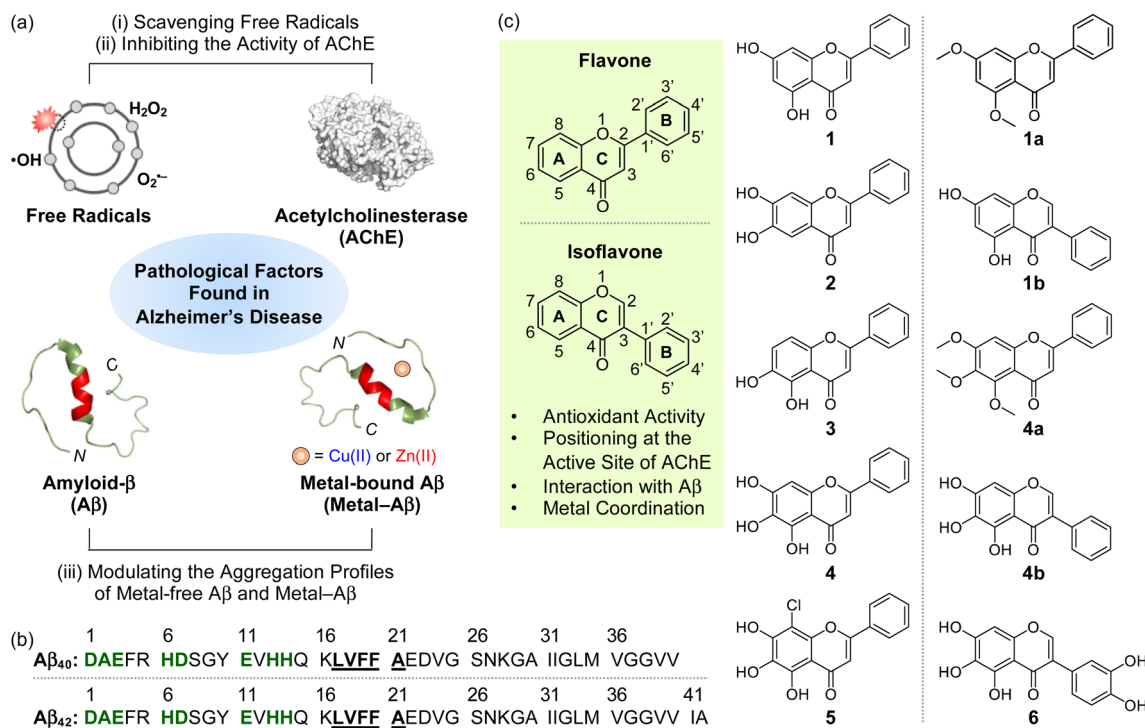


Fig. 1 Multiple pathogenic factors and flavonoids studied in this work. (a) Free radicals, AChE (PDB 1C2B<sup>64</sup>), metal-free Aβ (PDB 2LFM<sup>65</sup>), and metal-Aβ as pathological elements to be controlled in this work. (b) Sequences of Aβ peptides. Amino acid residues involved in the metal-binding and self-recognition sites are highlighted in bold/green and bold/underline, respectively. (c) Chemical structures of flavonoids 1–5, 1a, 1b, 4a, 4b, and 6. 1, chrysin; 2, 6,7-dihydroxyflavone; 3, 5,6-dihydroxyflavone; 4, baicalein; 5, 8-chlorobaicalein; 1a, 5,7-dimethoxyflavone; 1b, 5,7-dihydroxyisoflavone; 4a, 5,6,7-trimethoxyflavone; 4b, 5,6,7-trihydroxyisoflavone; 6, 3-(3,4-dihydroxyphenyl)-5,6,7-trihydroxy-4H-chromen-4-one.

desired pathological targets through systematic investigations. Moreover, a highly promising flavonoid with multiple functions was developed based on our structure–activity relationship analysis, with the determination of molecular-level mechanistic details. Our overall studies demonstrate the potential of flavonoids as multifunctional chemical reagents for AD and serve as a roadmap for the future development of multi-target-directed small molecules in the fight against neurodegenerative disorders, such as AD.

## Results and discussion

### Selection and preparation of flavonoids

Given that flavonoids as a family of naturally occurring polyphenols have antioxidant,<sup>37,38</sup> antiviral,<sup>39</sup> and antimicrobial activities,<sup>40</sup> we chose the flavonoid framework for our molecular design of small molecules with reactivities of multiple pathological targets. As presented in Fig. 1c, some structural moieties of flavonoids are reported to be important for modulating free radicals, AChE, metal-free Aβ, and metal-Aβ: (i) The unsaturated bond between C2 and C3 on the C ring of flavonoids could interact with the hydrophobic self-recognition (Leu17–Ala21) and C-terminal regions of Aβ that are essential for its aggregation process;<sup>41–44</sup> (ii) the 4-oxo functionality on the C ring as an oxygen (O) donor atom can participate in metal coordination;<sup>45</sup> (iii) the chromone moiety (A and C rings) is responsible for the reactivity of flavonoids against AChE through the interactions

with amino acid residues containing an aromatic ring at their side chains (e.g., Trp86, Phe295, and Tyr341) within the hydrophobic binding pocket of AChE;<sup>46</sup> (iv) both the number and position of hydroxyl groups are associated with chemical properties, such as redox potentials, hydrogen bonding, and aqueous solubility.<sup>47</sup>

In addition to the abovementioned structural features of flavonoids, the incorporation of hydroxyl groups on the B and C rings and the isoflavone variation to regulate pathological factors have been recently identified;<sup>45,46,48</sup> however, the information on structural and chemical properties on the A ring for multiple reactivities towards our desired targets, except for AChE,<sup>49</sup> is very limited. Thus, to gain a full spectrum of the structure–activity relationship with respect to all the A, B, and C rings, we rationally selected a series of nine flavonoids (1–5, 1a, 1b, 4a, and 4b; Fig. 1c) through the structural variation of functional groups on the A ring and translocation of the B ring from C2 to C3 that can alter their electronic and AChE/Aβ-interacting properties. Flavonoids 1–3 containing two hydroxyl groups located at distinct positions on the A ring were first chosen. Our series also included 4 possessing three hydroxyl groups on the A ring. Flavonoid 5 that embodies three hydroxyl groups with an electron-withdrawing chloro group at the C8 position on the A ring was additionally selected. Moreover, 1a/4a (substituted with methoxy groups instead of hydroxyl groups) and 1b/4b (isoflavone derivative), which originate from 1 and 4, respectively, were also included in our series. Flavonoids were



obtained from commercially available sources (**1–4**, **1a**, **1b**, and **4a**) or prepared following previously reported synthetic routes (**5**<sup>50</sup> and **4b**<sup>51</sup>). The characterization of **5** and **4b** was summarized in Fig. S1 and S2,<sup>†</sup> respectively. The investigations of how the structural variations of the flavonoids shown in Fig. 1c on the A ring alter their reactivities against multiple pathological factors, with previously reported structure–reactivity studies using a series of flavonoids chosen based on distinct structural modifications on the B and C rings,<sup>45,46,48</sup> led to the development of a promising multi-target-directed flavonoid (**6**; Fig. 1c) (*vide infra*).

### Redox potentials and scavenging free radicals

The redox activity of small molecules is critical for controlling multiple pathological features of AD, including free radicals, metal-free A $\beta$ , and metal–A $\beta$ .<sup>47,52–55</sup> In particular, redox properties of small molecules are connected with their antioxidant ability.<sup>56</sup> Thus, the redox potential of flavonoids were first computed following the previously reported density functional theory (DFT) calculation.<sup>57</sup> It should be noted that we could not experimentally obtain the flavonoids' redox potentials due to their instability and

limited solubility in aqueous or organic media used for their electrochemical measurements. As illustrated in Fig. 2a, the calculated redox potentials were varied with the number and position of electron-donating hydroxyl groups on the A ring. Based on the position of hydroxyl groups on the A ring shown in **1–3**, their  $E^\circ$  values *vs.* standard hydrogen electrode (SHE) were ranged from 1.440–1.534 V. In detail, the incorporation of two hydroxyl substituents *ortho*-positioned at either C6/C7 (**2**) or C5/C6 (**3**) decreased the redox potentials, relative to that at the *meta*-position (C5/C7, **1**). Furthermore, **4** with an additional hydroxyl group on the A ring revealed a lower redox potential; however, incorporating an electron-withdrawing chloro substituent at the C8 position of **4**, designated as **5**, yielded an similar level of  $E^\circ$  value comparable to that of **2** and **3**. The substitution of hydroxyl groups with methoxy moieties on the A ring, as presented in **1a/4a**, and the alteration of the position of the B ring, as shown in **1b/4b**, resulted in relatively higher and lower calculated  $E^\circ$  values, respectively, when compared to their respective parent structures (**1** and **4**).

To obtain a greater understanding of computed redox potentials, the highest occupied molecular orbitals (HOMOs) of **1–5**,

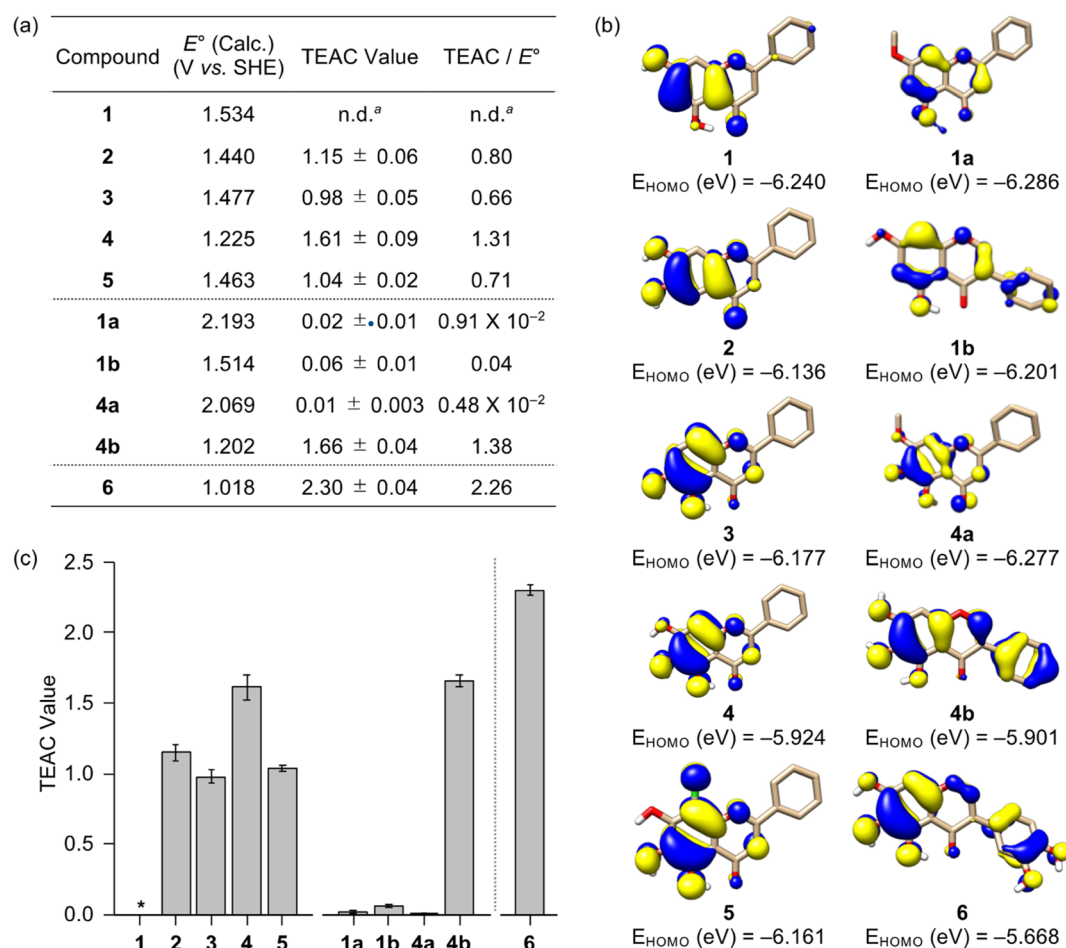


Fig. 2 Redox properties of flavonoids and their ability to quench free organic radicals. The (a) redox potentials ( $E^\circ$  vs. SHE) of the flavonoids were calculated with the (b) isosurface plots (isodensity value = 0.03 a.u.) of their HOMOs. (a and c) TEAC values of the flavonoids determined by the TEAC assay. Conditions: EtOH; 25 °C;  $\lambda_{\text{abs}} = 734$  nm. <sup>a</sup>n.d., not determined. \*Note that the TEAC value of **1** could not be obtained due to its limited solubility in EtOH.



**1a**, **1b**, **4a**, and **4b** were analyzed. As displayed in Fig. 2b, **1** exhibited the relatively low HOMO level among **1–5**, **1a**, **1b**, **4a**, and **4b**, which is correlated with the order of calculated  $E^\circ$  value. The orbital lobes localized at the C5–C7 positions in the HOMOs of **1–3** showed that electron-donating groups at those positions may effectively elevate the HOMO level. In good agreement with this expectation, the HOMO level of **4** carrying three hydroxyl groups at all the C5, C6, and C7 positions was reached at  $-5.924$  eV, which became lower (for **5**) when an electron-withdrawing moiety was located at the C8 position. In addition, the HOMO levels of **1a** and **4a** were relatively stabilized, compared to those of **1** and **4**, by an inductive effect from the *meta*-positioned methoxy substituents.<sup>58</sup> Moreover, the translocation of an electron-rich phenyl ring (B ring) from  $\delta^+$ -charged  $\beta$ -carbon (C2) to  $\delta^-$ -charged  $\alpha$ -carbon (C3) offered the higher HOMO levels of **1b** and **4b** due to the unfavorable  $\pi$ -conjugation on the C ring enone, relative to **1** and **4**, respectively.

To determine the ability of **1–5**, **1a**, **1b**, **4a**, and **4b** to quench free organic radicals, we performed the Trolox equivalent antioxidant capacity (TEAC) assay employing the cationic radical form of 2,2'-azino-bis(3-ethylbenzthiazoline-6-sulphonic acid).<sup>59</sup> As presented in Fig. 2a and c, flavonoids were tested, except for **1** that has limited solubility in ethanol (EtOH) under our experimental conditions. Flavonoids **2–5** and **4b** showed the TEAC values close or over 1.0, relative to a vitamin E analog Trolox, suggesting that their radical scavenging ability is similar or greater than that of Trolox. As expected from the calculated redox potentials shown in Fig. 2a, **1a**, **1b**, and **4a** presented no significant radical scavenging activity, relative to that of Trolox.

As anticipated from the calculated  $E^\circ$  values, relatively low TEAC values were observed for **2** and **3** over **4** and **4b**. This investigation manifests the significance of the number of hydroxyl groups on the A ring towards redox properties and antioxidant activity. Despite three hydroxyl groups on the A ring, **5** with an electron-withdrawing chloro group displayed a similar TEAC value with **2** and **3** containing two hydroxyl groups. Our computational and experimental studies confirm that the iso-flavone **4b** embodying three hydroxyl groups without an electron-withdrawing substituent on the A ring can have the lowest redox potential among **1–5**, **1a**, **1b**, **4a**, and **4b**, with the consequent noticeable radical scavenging ability. Moreover, the prooxidative activity of **2–5** and **4b** that exhibit a notable radical scavenging ability were further analyzed by a cell-based fluorescent ROS detection assay employing human neuroblastoma SH-SY5Y (5Y) cells. As presented in Fig. S3,<sup>†</sup> no elevation of the cellular ROS concentration upon incubation with 0.01 and 0.1 mM of **2–5** and **4b** was observed; however, as the increase of their concentrations, the prooxidative activity was observed at 0.5 and 1 mM. Such alteration in the antioxidant or prooxidant activity of flavonoids depending on their concentrations was reported in previous studies.<sup>37,38</sup> Collectively, these results suggest that flavonoids **2–5** and **4b** effectively scavenge free radicals, but they have the prooxidant activity under certain conditions, *e.g.*, high concentrations.

### Inhibition against AChE

Inhibiting the activity of AChE can maintain a proper level of ACh under dysregulated cholinergic conditions.<sup>10,11</sup> Thus, the

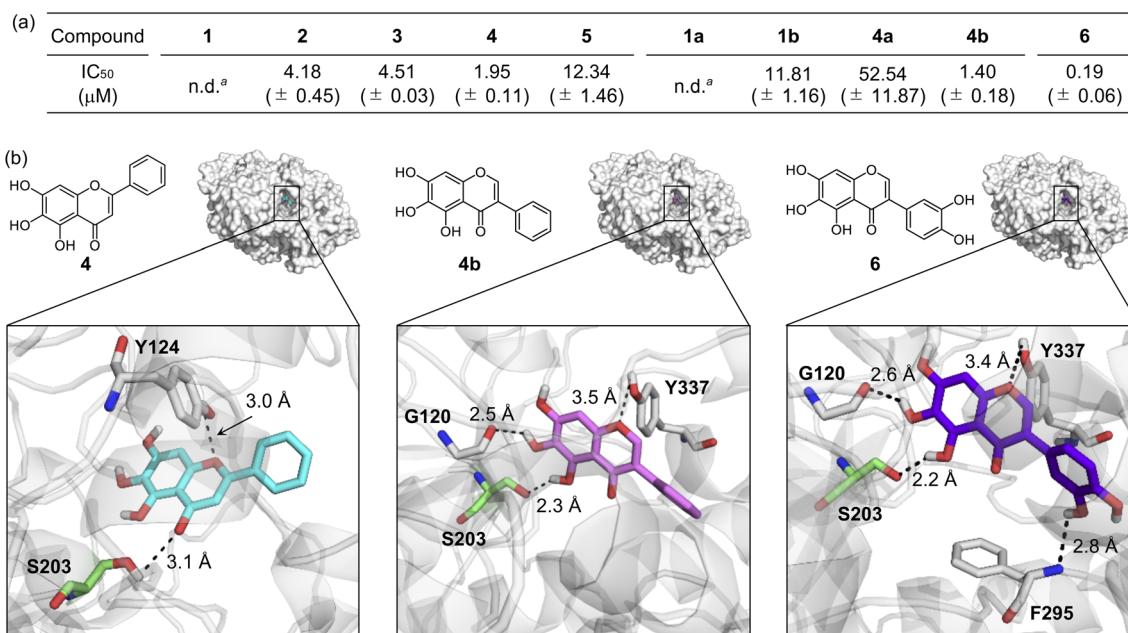


Fig. 3 Inhibitory ability of flavonoids against AChE. (a) IC<sub>50</sub> values of **1–5**, **1a**, **1b**, **4a**, **4b**, and **6** for AChE inhibition determined by a fluorometric assay. <sup>a</sup>n.d., not determined. Note that the IC<sub>50</sub> values of **1** and **1a** could not be obtained due to their low inhibitory activity against AChE. (b) Possible interactions of **4**, **4b**, and **6** with AChE (PDB 1C2B<sup>64</sup>) visualized by docking studies. Nine docked models of **4**, **4b**, and **6** against AChE with binding energies ranging from  $-10.8$  to  $-8.7$  kcal mol<sup>-1</sup> were obtained. The representative models with the highest binding affinity towards AChE are shown in the figure. Hydrogen bonds between the flavonoids and AChE are indicated with dashed lines (2.2–3.5 Å). N, O, H, and C (from Ser203) atoms are depicted in blue, red, white, and green, respectively.



inhibitory capability of flavonoids against AChE was investigated by a previously reported fluorescent AChE assay with slight modifications.<sup>60</sup> As summarized in Fig. 3a, the  $IC_{50}$  values of flavonoids were in a micromolar range ( $IC_{50} = 1.40\text{--}52.54 \mu\text{M}$ ). It should be noted that the  $IC_{50}$  values of **1** and **1a** could not be obtained due to their negligible inhibitory activity against AChE under our experimental conditions. **4** and **4b** that contain three hydroxyl groups on the A ring among our molecules exhibited relatively low  $IC_{50}$  values. The inclusion of three hydroxyl groups on the A ring is critical for controlling the catalytic activity of AChE, as previously reported,<sup>49</sup> whereas the incorporation of a chloro substituent, with three hydroxyl groups, and methoxy moieties instead of hydroxyl groups on the A ring can decrease such inhibitory activity. Flavonoids **2**, **3**, and **1b** over **1** illustrates the importance of the position of hydroxyl groups on the A ring and the isoflavone variation in directing the flavonoids' ability to inhibit the activity of AChE.

Docking studies were further conducted to visualize potential interactions between the flavonoids and AChE employing an X-ray crystal structure of electrophorus electricus AChE (PDB 1C2B<sup>61</sup>). As displayed in Fig. 3b and S4,<sup>†</sup> the flavonoids can interact with neighboring amino acid residues that lie in the active site of AChE *via* hydrogen bonding. For example, hydroxyl groups on the A ring could serve as a hydrogen-bond donor to interact with the backbone amide group between Gly121 and Gly122 (for **1** and **2**), the backbone carbonyl moiety of Gly120–Gly121 (for **3** and **4b**), and the hydroxyl group of Ser203 (for **4b**) in AChE. In addition, hydrogen bonds mediated by the central O donor atom and the 4-oxo functionality on the C ring with Tyr337/Tyr341 (for **1**, **2**, and **1a**), Gly122/Tyr124 (for **3**), Tyr124/Ser203 (for **4**), Tyr124 (for **5**), Tyr124/Tyr337 (for **1b**), Tyr124 (for **4a**), and Tyr337 (for **4b**) were also monitored. Anchoring the flavonoids into the cavity of the active site of AChE could prevent the substrate binding and, ultimately, inhibit the activity of AChE. In particular, hydrogen bonds between Ser203 at the catalytic triad and the 4-oxo functionality on the C ring of **4** or the hydroxyl group on the A ring of **4b** were indicated within 3.1 Å and 2.3 Å, respectively. The Ser203 residue is responsible for initiating the hydrolysis of ACh through hydrogen bonding;<sup>62</sup> thus, the intermolecular interaction with Ser203 could dominantly restrict ACh from binding into the active site of AChE. Overall, these observations highlight the pertinent role of some structural features, such as hydroxyl groups on the A ring and the C ring that contains two O donor atoms, in controlling the catalytic activity of AChE. It should be noted that the  $\pi$ – $\pi$  stacking between the flavonoids' chromone moiety (A and C rings) and amino acid residues at the anionic subsite of AChE could afford the stability for their positioning at the cavity of AChE's active site,<sup>46</sup> but our docking studies did not visualize these  $\pi$ – $\pi$  stacking interactions.

### Effects on A $\beta$ aggregation in the absence and presence of metal ions

To verify whether a series of nine flavonoids can modulate the aggregation of A $\beta$  with and without metal ions, the molecular weight (MW) distribution and morphology of the resultant A $\beta$

species were determined by gel electrophoresis with western blotting (gel/western blot) using an anti-A $\beta$  antibody (6E10) and transmission electron microscopy (TEM), respectively. Two types of experiments were carried out employing two major A $\beta$  isoforms, *i.e.*, A $\beta_{42}$  and A $\beta_{40}$ .<sup>25</sup> (i) inhibition studies to identify the effect of **1–5**, **1a**, **1b**, **4a**, and **4b** on the formation of A $\beta$  aggregates; (ii) disaggregation studies to evaluate if the flavonoids with reactivities towards A $\beta$  aggregation in inhibition studies can disassemble preformed A $\beta$  aggregates or modulate their further aggregation, as illustrated in Fig. 4 and S5–S9.<sup>†</sup> Moreover, the solutions containing the flavonoids and Cu(II) were probed by electronic absorption (Abs) spectroscopy to monitor their metal binding. As depicted in Fig. S10,<sup>†</sup> when **1–5**, **1b**, and **4b** were incubated with 1 equiv. of Cu(II), optical shifts corresponding to Cu(II) binding to the O donor atoms, *e.g.*, the hydroxyl groups at the C5–C7 positions and the 4-oxo functionality on the A and C rings of the flavonoids, respectively (Fig. 1c). As expected, no Abs change of **1a** and **4a** composed of methoxy groups on the A ring was detected by addition of Cu(II).

As presented in Fig. 4b, S5a, and S9a,<sup>†</sup> the inhibition experiments with metal-free A $\beta_{42}$  showed the notably varied MW distribution upon treatment of **4**, **5**, and **4b** over **1–3**, **1a**, **1b**, and **4a**. Flavonoids **4**, **5**, and **4b** discernably reduced the signal intensity of the bands corresponding to A $\beta_{42}$  with the MWs from *ca.* 4–20 kDa and larger than *ca.* 100 kDa, while **1–3**, **1a**, **1b**, and **4a** could not change the size distribution of metal-free A $\beta_{42}$ . In the case of Cu(II)–A $\beta_{42}$  incubated with **3** over compound-untreated Cu(II)–A $\beta_{42}$  or Cu(II)–A $\beta_{42}$  added with **1**, **2**, **1a**, **1b**, and **4a**, more intense smearing was monitored in the MW window larger than *ca.* 25 kDa. The sample of Cu(II)–A $\beta_{42}$  incubated with **4** displayed the enhanced level of dodecameric or larger A $\beta_{42}$  aggregates (*ca.*  $\geq 50$  kDa), with the decreased intensity of the bands assigned to monomeric, dimeric, trimeric, and tetrameric A $\beta_{42}$ . The alteration of the size distribution of Cu(II)–A $\beta_{42}$  induced by **5** and **4b** was similar to that by the addition of **3**. Comparable to Cu(II)–A $\beta_{42}$ , the size distribution of Zn(II)–A $\beta_{42}$  species was modified by **4**, **5**, and **4b**, with the indication of smearing bands at *ca.* 25–240 kDa, while **3** gave rise to increased signal intensity between *ca.* 25–75 kDa. In contrast, a significant change in the MW distribution was not indicated by addition of **1**, **2**, **1a**, **1b**, and **4a**.

TEM investigations further supported the flavonoids' reactivity towards the aggregation of A $\beta_{42}$ . As illustrated in Fig. 4b and S5b,<sup>†</sup> the resultant metal-free A $\beta_{42}$  aggregates produced with **4**, **5**, and **4b** exhibited noticeably different morphologies from compound-untreated A $\beta_{42}$  aggregates, while little or no morphological alteration was observed from those incubated with **1–3**, **1a**, **1b**, and **4a**. Metal-free A $\beta_{42}$  added with **4** generated shorter and thinner fibrils. Upon incubation of **5** and **4b** with metal-free A $\beta_{42}$  species, smaller fibrils and less structured aggregates were monitored than those obtained from compound-unadded metal-free A $\beta_{42}$ , which was supported by circular dichroism (CD) spectroscopic investigations. When metal-free A $\beta_{42}$  was treated with **5** or **4b** for 24 h, a decrease in the  $\beta$ -sheet population [for **5**, 66.7 ( $\pm 15.3$ )%; for **4b**, 35.5 ( $\pm 5.7$ )%] and increase in the random-coil feature [for **5**, 19.7 ( $\pm 15.5$ )%; for **4b**, 53.8 ( $\pm 5.9$ )%] were monitored, compared to



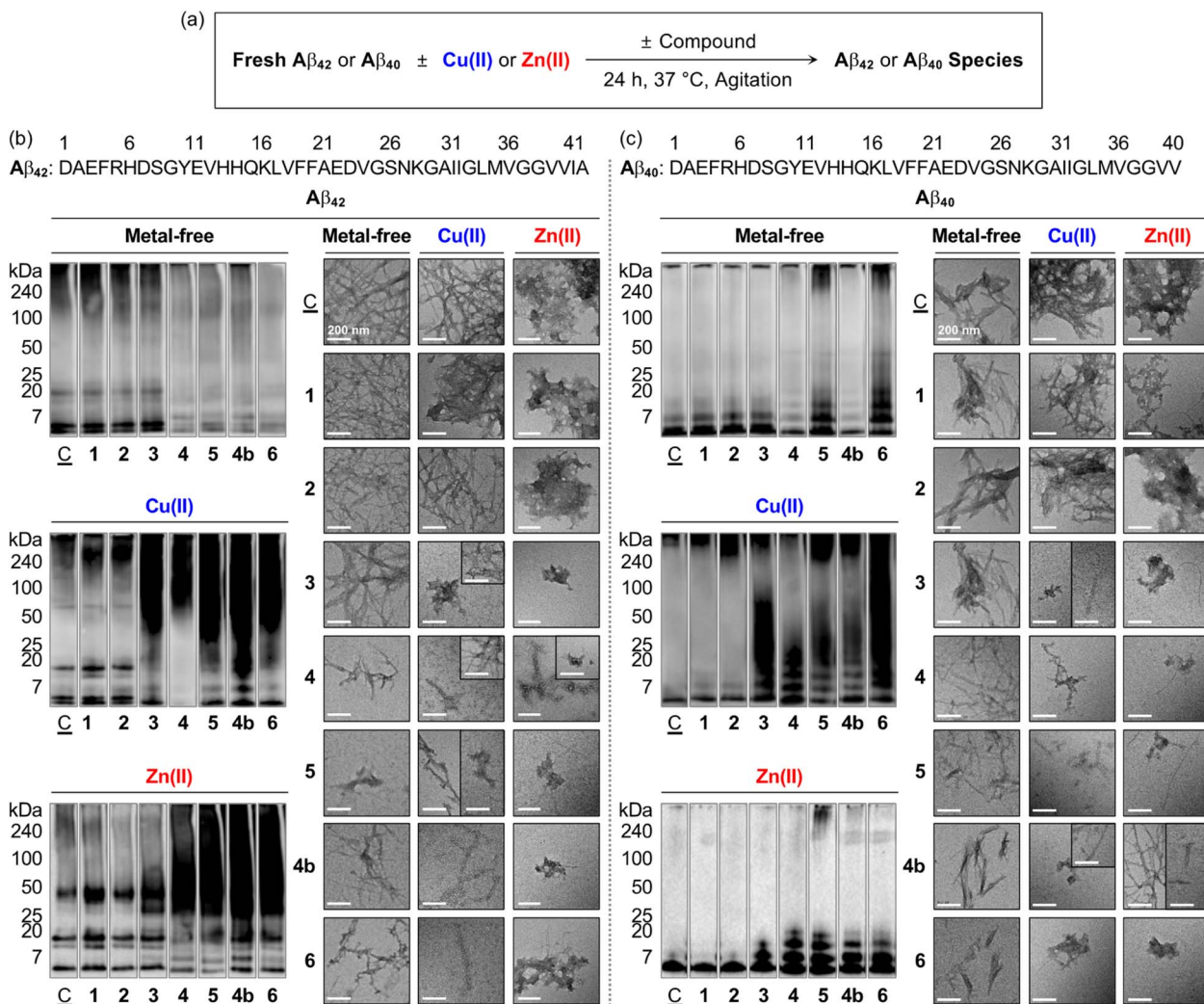


Fig. 4 Effects of 1–6 and 4b on the formation of metal-free  $\text{A}\beta$  and metal– $\text{A}\beta$  aggregates. (a) Scheme of the inhibition experiments. MW distributions and morphologies of the resultant (b)  $\text{A}\beta_{42}$  and (c)  $\text{A}\beta_{40}$  species were analyzed by gel/western blot with an anti- $\text{A}\beta$  antibody (6E10) and TEM, respectively. Lanes: (C)  $\text{A}\beta \pm \text{Cu(II) or Zn(II)}$ ; (1) C + 1; (2) C + 2; (3) C + 3; (4) C + 4; (5) C + 5; (4b); C + 4b; (6) C + 6. The original gel images are shown in Fig. S9a.† Conditions:  $[\text{A}\beta] = 25 \mu\text{M}$ ;  $[\text{M(II)}] = 25 \mu\text{M}$ ;  $[\text{flavonoid}] = 50 \mu\text{M}$  (1% v/v DMSO); 20 mM HEPES, pH 7.4, 150 mM NaCl;  $37^\circ \text{C}$ ; 24 h; constant agitation. Scale bars = 200 nm.

those of the compound-untreated sample [ $\beta$ -sheet, 73.7 ( $\pm 0.7$ )%; random coils, 1.5 ( $\pm 1.5$ )%] (Fig. S11†). In the case of  $\text{Cu(II)}\text{-A}\beta_{42}$ , 3–5 and 4b could vary the morphology of the resultant aggregates. A mixture of amorphous and small fibrillary aggregates was detected upon incubation of 3 and 5 with  $\text{Cu(II)}\text{-A}\beta_{42}$ , relative to mature fibrils observed upon incubation of  $\text{Cu(II)}\text{-A}\beta_{42}$  only. The samples of  $\text{Cu(II)}\text{-A}\beta_{42}$  with 4 and 4b showed chopped and thin fibrils. The resultant aggregates of  $\text{Zn(II)}\text{-A}\beta_{42}$  were notably different by treatment of 3–5 and 4b, compared to large amorphous species observed in the sample of  $\text{Zn(II)}\text{-A}\beta_{42}$  only. Flavonoids 3 and 4b triggered the formation of small amorphous aggregates. The addition of 4 to  $\text{Zn(II)}\text{-A}\beta_{42}$  led to the generation of chopped fibrils and amorphous assemblies. In the presence of 5, both amorphous and fibrillary  $\text{Zn(II)}\text{-A}\beta_{42}$  aggregates were monitored. Flavonoids 1, 2, 1a, 1b, and 4a did not indicate any noticeable morphological changes of the resultant  $\text{Cu(II)}\text{-A}\beta_{42}$  and  $\text{Zn(II)}\text{-A}\beta_{42}$  aggregates.

Moreover, to investigate the effects of the flavonoids on the oligomerization and fibrilization of metal-free  $\text{A}\beta_{42}$  and metal– $\text{A}\beta_{42}$ , we performed the dot blot assay employing anti-oligomer (A11) and anti-fibril (OC) antibodies,<sup>23</sup> as illustrated in Fig. S12.† It should be noted that the thioflavin-T (ThT) assay utilized for monitoring the formation of  $\beta$ -sheet-rich aggregates cannot be carried out under our experimental conditions since the absorption windows of 4, 5, and 4b interfere with the excitation and emission wavelengths of ThT (Fig. S13†). As expected from our gel/western blot and TEM studies (*vide supra*), A11- and OC-detectable immunofluorescent signals were not significantly varied by treatment of 1, 2, 1a, 1b, and 4a with metal-free  $\text{A}\beta_{42}$  and metal– $\text{A}\beta_{42}$  following incubation, relative to those from compound-untreated samples (Fig. S12†). In contrast, the formation of  $\text{A}\beta$  oligomers and fibrils were reduced in the samples of metal-free  $\text{A}\beta_{42}$  treated with 4, 5, and 4b, following 24 h incubation. In the case of  $\text{Cu(II)}\text{-A}\beta_{42}$  or  $\text{Zn(II)}\text{-A}\beta_{42}$ , 3–5



and **4b** showed the gradually decreased signal intensities detected by A11 and OC in a distinctive manner, indicative of the modulatory ability of **3–5** and **4b** against the oligomerization and fibrilization of metal- $A\beta_{42}$ .

The aggregation of metal-free  $A\beta_{40}$  and metal- $A\beta_{40}$  could be modified by flavonoids in a different extent to that observed with metal-free and metal-added  $A\beta_{42}$ . As illustrated in Fig. 4c, S6, and S9a,† under metal-free conditions, the signal intensity of the bands from *ca.* 7–20 kDa assigned to smaller oligomeric  $A\beta_{40}$  species was reduced by **4** and **4b**, while **5** increased the band intensity associated with the species larger than *ca.* 7 kDa. When **3–5** and **4b** were treated to  $Cu(II)-A\beta_{40}$  and  $Zn(II)-A\beta_{40}$ , the resultant  $A\beta$  species indicated the diverse MW distribution in the range of *ca.* 7–240 kDa to different extents. As shown in TEM images, shorter and thinner fibrils were generated in the samples of metal-free  $A\beta_{40}$  with **4**, **5**, and **4b**. For  $Cu(II)-A\beta_{40}$ , **5** formed chopped filamentous  $Cu(II)-A\beta_{40}$  aggregates, and **3**, **4**, and **4b** produced both amorphous and fibrillary aggregates. These morphological changes were similar to those of  $Zn(II)-A\beta_{40}$  incubated with **3–5** and **4b** generated a bunch of fibrillary species with chopped filamentous aggregates.

Moreover, the disaggregation experiments exhibited the effects of **1–5** and **4b** on preformed  $A\beta_{42}$  and  $A\beta_{40}$  aggregates in the absence and presence of  $Cu(II)$  and  $Zn(II)$ , as summarized in Fig. S7 and S9b.† Flavonoids **4**, **5**, and **4b** could disassemble preformed metal-free  $A\beta$  and metal- $A\beta$  aggregates. In the case of **3**, the reactivity was shown only in the presence of metal ions. Flavonoids **1** and **2** less noticeably affected preformed metal-free and metal-treated  $A\beta$  aggregates. To probe the secondary nucleation of disassembled  $A\beta$  aggregates induced by the flavonoids on  $A\beta$  monomers, additional disaggregation experiments were conducted by incubating preformed aggregates of metal-free and metal-treated  $A\beta$  or their seeds with  $A\beta$  monomers. As shown in Fig. S8,† **4**, **5**, and **4b** exhibited notable variations in the MW distribution of both metal-free  $A\beta_{42}$  and metal- $A\beta_{42}$  species, and **3** displayed the reactivity specifically towards metal- $A\beta_{42}$  species. These findings suggest that the generated  $A\beta$  fragments by the flavonoids could suppress secondary nucleation. Collectively, our overall inhibition and disaggregation studies demonstrate that **4**, **5**, and **4b** can modulate the aggregation of  $A\beta$  in the absence and presence of metal ions as well as disassemble preformed metal-free  $A\beta$  and metal- $A\beta$  aggregates. In contrast, among the flavonoids containing two hydroxyl or two/three methoxy groups on the A ring, **3** exhibits the corresponding reactivities only towards metal-mediated  $A\beta$  aggregation pathways. These indications describe the significance of three hydroxyl groups on the A ring in the flavonoid structure to impact the aggregation of metal-free  $A\beta$  and metal- $A\beta$ .

### Rational selection, redox potential, synthesis, and cytotoxicity of **6**

Based on the structure–activity relationship observed employing a series of nine flavonoids (Fig. 1c) with the previously reported studies of flavonoids,<sup>46,48,49</sup> we could determine structural features on all the A, B, and C rings of flavonoids that

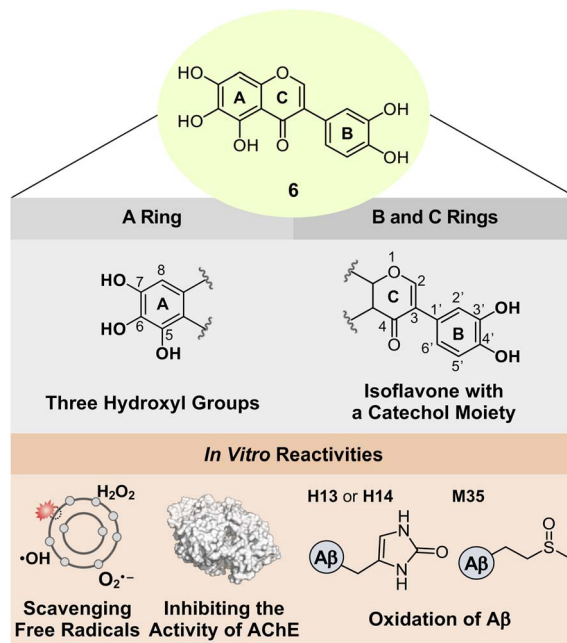


Fig. 5 Design rationale of **6** and its reactivities against free radicals, AChE, metal-free  $A\beta$ , and metal- $A\beta$ .

are critical for controlling multiple pathological factors, *i.e.*, free radicals, AChE, metal-free  $A\beta$ , and metal- $A\beta$ . As depicted in Fig. 5, first, three hydroxyl groups at the C5–C7 positions on the A ring are essential for gaining multiple reactivities with our desired pathogenic targets, relative to that of two hydroxyl or two/three methoxy groups. Second, the translocation of the B ring from C2 to C3 on the C ring, which produces an isoflavone framework, can enhance both free radical scavenging and AChE inhibitory activities. Third, a catechol moiety on the B ring in an isoflavone backbone is reported to be important in modulating the reactivities of our targets.<sup>46</sup> In particular, a catechol group has been widely used for the design of chemical reagents (*e.g.*, small molecules and nanomaterials) as inhibitors against  $A\beta$  aggregation.<sup>45,63–65</sup> Moreover, as illustrated in Fig. 2b, comparing the HOMOs of **4** and **4b** indicates that the electronic distribution on all the A, B, and C rings is notable in the isoflavone **4b**; thus, the addition of electron-donating groups at the C3' and C4' positions on the B ring can impact the electronic property of the overall structure. Collectively, we rationally fashioned the isoflavone **6** (Fig. 5) that contains three hydroxyl groups on the A ring and a catechol moiety on the B ring, as a flavonoid with multiple reactivities against pathological components in AD. As expected, **6** showed the most negative redox potential among all flavonoids, as shown in Fig. 2a. The addition of a catechol moiety on the B ring onto the isoflavone framework of **4b** containing three hydroxyl groups on the A ring lowered the calculated redox potential from 1.202 to 1.018 V (*vs.* SHE). The orbital lobes localized between C3' and C4' in the HOMO of **6** can rationalize its more elevated HOMO level with the subsequent negative calculated  $E^\circ$  value, compared to that of **4b**, as displayed in Fig. 2a and b.





Scheme 1 Synthetic routes to **6**.

Flavonoid **6** was synthesized following previously reported procedures with modifications.<sup>66–68</sup> As presented in Scheme 1 and Fig. S14–S16,<sup>†</sup> the Friedel–Crafts acylation of **6a** with **6b** afforded **6c** in the presence of boron trifluoride ethyl etherate ( $\text{BF}_3\cdot\text{OEt}_2$ ) as both the catalyst and solvent. Flavonoid **6d** was prepared by the subsequent cyclization reaction of **6c** using methanesulfonyl chloride ( $\text{MeSO}_2\text{Cl}$ ), and the final product **6** was obtained *via* the demethylation reaction of **6d** with boron tribromide ( $\text{BBr}_3$ ). After the preparation, the cytotoxicity of **6**, compared to **1–5** and **4b**, was determined by 3-(4,5-dimethylthiazol-2-yl)-2,5-diphenyltetrazolium bromide (MTT) assay employing human neuroblastoma 5Y cells. As summarized in Fig. S17,<sup>†</sup> greater than *ca.* 90% survival at up to 100  $\mu\text{M}$  was observed upon the cells treated with **6** for 24 h. In contrast, the cells upon incubation with 100  $\mu\text{M}$  of **1–5** and **4b** indicated *ca.* 30%, 60%, 50%, 70%, 60%, and 70% viability, respectively, suggesting that **6** over **1–5** and **4b** has relatively low cytotoxicity. It should be noted that cell viability was calculated, relative to that of the cells containing an equivalent amount of DMSO.

### Reactivities of **6** with free organic radicals, AChE, metal-free A $\beta$ , and metal–A $\beta$

Flavonoid **6** exhibited the significant scavenging capability towards free organic radicals with the highest TEAC value [2.30 ( $\pm 0.04$ )] among our flavonoid series, as shown in Fig. 2a and c. No prooxidative activity of **6** at up to 0.1 mM was observed; however, the cells upon incubation with 0.5 and 1 mM of the flavonoid indicated an increase in the amount of cellular ROS (Fig. S3<sup>†</sup>). These results imply that **6** serves as an antioxidant or prooxidant depending on experimental conditions. In addition, the most remarkable inhibition against the activity of AChE was observed by **6** with a nanomolar  $\text{IC}_{50}$  value (Fig. 3a). To visualize the potential interactions of **6** with AChE, docking studies were conducted. As illustrated in Fig. 3b, three and two hydroxyl groups on the A and B rings, respectively, and the central O donor atom on the C ring could have hydrogen bonds with the backbone carbonyl moiety of Gly120–Gly121, the hydroxyl group of Ser203 and Tyr337, and the backbone amide group between Ile294 and Phe295 within the cavity of AChE's active site.

Especially, a hydrogen bond between the hydroxyl group at the C5 position on the A ring and Ser203 at the catalytic triad was indicated within 2.2 Å. Moreover, the number of hydrogen bonds between **6** and amino acid residues in the substrate-binding pocket of AChE was increased to four, as expected from the additional catechol functionality on the B ring, compared to that shown in **1–5**, **1a**, **1b**, **4a**, and **4b** [one (for **4a** and **5**); two (for **1a**, **1b**, and **4**); three (for **1–3** and **4b**)]. These overall interactions can position **6** in the cavity of the active site and sterically halt the substrate ACh binding into the catalytic triad, which leads to its noticeable inhibitory ability against the activity of AChE.

Moving forward, **6** remarkably modified the oligomerization and fibrillization of both metal-free A $\beta$  and metal–A $\beta$  and affected their corresponding preformed A $\beta$  aggregates and seeds, with its Cu(II)-binding property, as illustrated in Fig. 4 and S7–S12.<sup>†</sup> In the inhibition experiments (gel/western blots), the intensity of the bands from the sample containing **6** and metal-free A $\beta_{42}$  was reduced at *ca.* 4–20 kDa and above *ca.* 100 kDa, relative to that observed in the compound-free sample (Fig. 4b and S9a<sup>†</sup>). Furthermore, smearing bands from *ca.* 20–240 kDa were noticeably detected upon incubation of Cu(II)–A $\beta_{42}$  and Zn(II)–A $\beta_{42}$  with **6**. TEM studies indicated shorter and thinner fibrils by adding **6** with metal-free A $\beta_{42}$  than those of compound-untreated metal-free A $\beta_{42}$ . This result was supported by the CD analysis that indicated a change in the secondary structure of metal-free A $\beta_{42}$  in the presence of **6**, relative to that of the compound-free sample (Fig. S11<sup>†</sup>). The morphological changes of Cu(II)–A $\beta_{42}$  and Zn(II)–A $\beta_{42}$  aggregates were also prominent upon treatment of **6**, exhibiting chopped fibrils and a mixture of amorphous and fibrillary aggregates, respectively (Fig. 4b). These reactivities of **6** were further supported by the dot blot assay, indicating significantly decreased A11- and OC-detectable signal intensities (Fig. S12<sup>†</sup>). The modulatory abilities of **6** were also observed in the inhibition studies with A $\beta_{40}$  (Fig. 4c and S9a<sup>†</sup>) as well as the disaggregation experiments employing preformed metal-free and metal-bound A $\beta_{42}$  and A $\beta_{40}$  aggregates (Fig. S7, S8, and S9b<sup>†</sup>).

### Interaction of **6** towards A $\beta$

Distinct reactivities of **6** with metal-free A $\beta$  and metal–A $\beta$  were supported by various biophysical approaches. As displayed in Fig. S18,<sup>†</sup> the chemical transformation of **6** triggered by metal-free A $\beta_{40}$  or metal–A $\beta_{40}$  was detected by Abs spectroscopy. In the absence of A $\beta$ , an increase or decrease in the absorption of the peaks at *ca.* 265, 300, 340, and 410 nm was monitored for 24 h (Fig. S18<sup>†</sup>), which could be resulted from the oxidation of **6** in the presence of  $\text{O}_2$ .<sup>69</sup> These spectral changes were accelerated upon incubation with A $\beta$ , indicative of its impact on the oxidative modification of **6**. Such transformation of **6** was also indicated in the presence of Cu(II) or Zn(II) with and without A $\beta$ . To probe the interaction of **6** with A $\beta$ , their binding properties were analyzed by isothermal titration calorimetry (ITC). For the association between **6** and A $\beta$ , we recorded the heat change upon constant titration of the flavonoid into the solution of A $\beta$ , where the dilution heat was also measured to avoid the heat





**Fig. 6** Interaction of **6** with monomeric  $\text{A}\beta_{42}$ . (a) Binding of **6** with  $\text{A}\beta_{42}$  recorded by ITC. The ITC thermogram (left) and binding isotherm (right) of **6** with  $\text{A}\beta_{42}$  are depicted. The solid line indicates the best fit of the ITC data to a one-site binding model. Conditions:  $[\text{A}\beta_{42}] = 40 \mu\text{M}$ ;  $[\text{6}] = 800 \mu\text{M}$  (1% v/v DMSO); 20 mM HEPES, pH 7.4; 10 °C. (b)  $2\text{D } ^1\text{H}-^{15}\text{N}$  SOFAST-HMQC NMR (800 MHz) spectra of  $^{15}\text{N}$ -labeled  $\text{A}\beta_{42}$  incubated with and without **6**. (c) CSPs and peak intensity ratios of amino acid residues in  $^{15}\text{N}$ -labeled  $\text{A}\beta_{42}$  upon treatment of **6**. Amino acid residues involved in the  $\beta$ -turn motif and the self-recognition site are highlighted in bold/green and bold/underline, respectively. The unresolvable peaks (*i.e.*, Asp1, Arg5, His6, His14, Val24, and Asn27) are indicated with asterisks. Two horizontal lines indicate the average chemical shift (solid line) plus one standard deviation (dashed line). Conditions:  $[^{15}\text{N}$ -labeled  $\text{A}\beta_{42}] = 33 \mu\text{M}$ ;  $[\text{6}] = 100 \mu\text{M}$  (1% v/v DMSO); 20 mM HEPES, pH 7.4; 10% v/v  $\text{D}_2\text{O}$ ; 10 °C.

change induced by its addition into the buffered solution. The complex of **6** and  $\text{A}\beta_{42}$  or  $\text{A}\beta_{40}$  was formed spontaneously and exothermically [for  $\text{A}\beta_{42}$ ,  $\Delta G = -6.1 (\pm 0.1) \text{ kcal mol}^{-1}$ ;  $\Delta H = -0.5 (\pm 0.1) \text{ kcal mol}^{-1}$ ;  $T\Delta S = 5.6 (\pm 0.1) \text{ kcal mol}^{-1}$ ; for  $\text{A}\beta_{40}$ ,  $\Delta G = -6.0 (\pm 0.5) \text{ kcal mol}^{-1}$ ;  $\Delta H = -0.6 (\pm 0.5) \text{ kcal mol}^{-1}$ ;  $T\Delta S = 5.4 (\pm 0.7) \text{ kcal mol}^{-1}$ ], which was driven by both negative enthalpy and positive entropy changes, as summarized in Fig. 6a and S19a.† Binding affinities of **6** towards  $\text{A}\beta_{42}$  and  $\text{A}\beta_{40}$  were determined to be *ca.* 19.5 ( $\pm 0.7$ ) and 20.5 ( $\pm 16.0$ )  $\mu\text{M}$ , respectively. Thus, **6** can bind to  $\text{A}\beta$  with a micromolar binding affinity.

The amino acid residues in  $\text{A}\beta$  affected upon interaction with **6** were further investigated by two-dimensional band selective optimized flip-angle short transient-heteronuclear multiple quantum correlation nuclear magnetic resonance (2D SOFAST-HMQC NMR) spectroscopy employing both  $^{15}\text{N}$ -labeled  $\text{A}\beta_{42}$  and  $\text{A}\beta_{40}$ . As presented in Fig. 6b and c, the chemical shift perturbations (CSPs) provoked by adding **6** to uniformly  $^{15}\text{N}$ -labeled  $\text{A}\beta_{42}$  were detected. The Gln15, Phe19, Gly33, and Leu34 residues in  $\text{A}\beta_{42}$  were changed by treatment of **6**, which implies that the flavonoid could affect the amino acid residues adjacent to the  $\beta$ -turn motif (Val12–Gln15), self-recognition site (Leu17–Ala21), and C-terminal region (Ile32–Ala42) of  $\text{A}\beta_{42}$  that are highly linked to its fibrilization.<sup>9,70–73</sup> Therefore, this interaction between **6** and  $\text{A}\beta_{42}$  could cause a change in the conformation and aggregation propensity of  $\text{A}\beta_{42}$ . Moreover,

the overall peak intensity of  $^{15}\text{N}$ -labeled  $\text{A}\beta_{42}$  was decreased by *ca.* 20% upon addition of **6**, suggesting the production of NMR-invisible  $\text{A}\beta$  aggregates.<sup>74</sup> In the case of  $\text{A}\beta_{40}$ , 2D SOFAST-HMQC NMR spectra obtained from  $^{15}\text{N}$ -labeled  $\text{A}\beta_{40}$  with and without **6** manifested the flavonoid's plausible interactions with Glu3, Glu11, Phe20, and Leu34 with the reduced overall peak intensity (*ca.* 10%), as depicted Fig. S19b and c.† In a similar manner to  $\text{A}\beta_{42}$ , **6** could alter the aggregation of  $\text{A}\beta_{40}$  by interacting with the aforementioned regions, including the self-recognition (Leu17–Ala21) and C-terminal (Ile32–Val40) sites.<sup>9,70–73</sup>

### $\text{A}\beta$ oxidation by **6**

To identify the modifications of  $\text{A}\beta$  in both the absence and presence of  $\text{Cu}(\text{II})$  upon treatment of **6**, we carried out the studies employing electrospray ionization mass spectrometry (ESI-MS). In the sample containing metal-free  $\text{A}\beta_{42}$  and **6**, the addition of +16 Da into the +3-charged  $\text{A}\beta_{42}$  monomer, assigned to be the oxidized monomeric  $\text{A}\beta_{42}$ , was detected (Fig. 7a), while such oxidation was not observed under anaerobic conditions (Fig. S20†). To determine the oxidized amino acid residues in  $\text{A}\beta_{42}$ , the *b* fragments generated by collision-induced dissociation were analyzed by tandem MS (ESI-MS<sup>2</sup>). As illustrated in Fig. 7b and S21a,† the Met35 residue was measured to be the oxidation site in the singly oxidized  $\text{A}\beta_{42}$ . The previous studies suggested that the His, Tyr, and Met residues in  $\text{A}\beta$  are susceptible to be oxidized and such oxidation could impact the



Fig. 7 Analysis of metal-free and Cu(II)-treated A $\beta_{42}$  upon addition of **6** by ESI-MS and ESI-MS<sup>2</sup>. ESI-MS spectra of +3-charged A $\beta_{42}$  and ESI-MS<sup>2</sup> analyses of the singly oxidized A $\beta_{42}$  (1511 m/z) were obtained upon incubation with **6** in the (a and b) absence and (c and d) presence of Cu(II). The peaks highlighted as a red circle correspond to the singly oxidized A $\beta_{42}$ . Detailed analysis of tandem spectra is summarized in Fig. S21.† Conditions: [A $\beta_{42}$ ] = 100  $\mu$ M; [Cu(II)] = 100  $\mu$ M; [**6**] = 200  $\mu$ M (1% v/v DMSO); 20 mM ammonium acetate, pH 7.4; 37 °C; 3 h; constant agitation. The samples were diluted by 10-fold with H<sub>2</sub>O before injection into the mass spectrometer.

aggregation profile of A $\beta$ .<sup>75–78</sup> In particular, the oxidation of the Met residue to Met sulfoxide or sulfone can increase its polarity leading to the destabilization of  $\beta$ -strand structures and the decrease in hydrophobic contacts onto the C-terminal region that are associated with amyloid aggregation.<sup>76,78</sup> Similar to metal-free A $\beta_{42}$ , the oxidation of A $\beta_{40}$  at the Met35 residue was monitored by incubation with **6** (Fig. S22a, b and S23a†).

A $\beta$  was oxidatively modified by incubation of Cu(II)-A $\beta$  with **6** in the presence of O<sub>2</sub> in a distinct manner from metal-free A $\beta$  treated with **6** (Fig. 7 and S20–S23†). As shown in Fig. 7c and S22c,† the intensity of the peaks assigned to Cu(II)-A $\beta_{42}$  and Cu(II)-A $\beta_{40}$  was suppressed. When collisional energy was selectively applied to the singly oxidized A $\beta$  produced by reacting Cu(II)-A $\beta$  with **6**, the analysis of *b* fragments indicated the His13, His14, and Met35 residues as plausible oxidation sites, as illustrated in Fig. 7d, S21b, S22d, and S23b.† In the case of His residues, their imidazole ring can involve in several intermolecular interactions, such as hydrogen bonding and  $\pi$ - $\pi$  stacking, as the hydrogen-bond donor/acceptor and an aromatic  $\pi$ -motif.<sup>79</sup> In addition, depending on pH, protonated His at both  $\epsilon$ - and  $\delta$ -nitrogen can mediate in the cation- $\pi$  interactions with aromatic amino acid residues (*e.g.*, Tyr and Phe) as well as the formation of an intramolecular salt bridge between the carboxylate group of Glu22 and the protonated His13 or His14.<sup>79–81</sup> Furthermore, His residues (*i.e.*, His6, His13, and His14) are included in metal coordination,<sup>5,82</sup> thus, the transformation of His to 2-oxo-His could disrupt intermolecular and intramolecular interactions within A $\beta$  and its metal binding.<sup>9,81,83</sup> It should be noted that Cu(II) chelation by **6** can

impact metal-binding properties of A $\beta$ .<sup>45</sup> Therefore, oxidative modifications onto His13, His14, and Met35 by **6** could modify the aggregation of Cu(II)-A $\beta$ . Together, our overall biophysical results and observations demonstrate the direct interactions of **6** with metal-free and metal-treated A $\beta$  species, with the consequent modulatory effects on their aggregation.

## Conclusions

AD is a complex condition, with multiple pathological factors contributing to its progression. This study presents a novel approach to developing flavonoids that can simultaneously target and regulate these factors. We conducted a series of experiments to identify key structural features for flavonoids to effectively control pathological targets and established the relationship between structure and activity. A series of nine flavonoids (**1–5**, **1a**, **1b**, **4a**, and **4b**) was rationally selected by adjusting the number and position of functional groups on the A ring and the position of the B ring, and their regulatory abilities against multiple pathogenic targets, including free radicals, AChE, metal-free A $\beta$ , and metal-A $\beta$ , were evaluated to establish the structure-activity relationship. Our investigations revealed three hydroxyl groups on the A ring as a critical structure feature to noticeably quench free organic radicals, inhibit the activity of AChE, and modulate the aggregation of metal-free A $\beta$  and metal-A $\beta$ . According to the structure-activity relationships obtained from this work (for the A ring) and the previous studies (for the B and C rings),<sup>46</sup> we strategically fashioned the isoflavone **6** possessing three hydroxyl groups on



the A ring and a catechol moiety on the B ring. Multiple reactivities of **6** against our desired targets are summarized: (i) scavenging free organic radicals exhibiting the highest TEAC value among our series of flavonoids; (ii) inhibiting the catalytic activity of AChE with a nanomolar IC<sub>50</sub> value; (iii) modifying the formation of metal-free Aβ and metal-Aβ aggregates; (iv) disassembling preformed Aβ aggregates and altering their further aggregation with and without metal ions. Moreover, our computational and biophysical studies illuminated mechanistic details of **6**'s versatile reactivities towards free organic radicals, AChE, metal-free Aβ, and metal-Aβ. A relatively low redox potential and structure-based interactions with the cleft at the active site of AChE offer significant free radical scavenging and AChE inhibitory capabilities of **6**, respectively. Oxidative modifications of metal-free and metal-added Aβ through direct interactions of **6** lead to altering their aggregation profiles. Our overall findings highlight a multidisciplinary strategic approach for designing multi-target-directed flavonoids as chemical reagents for AD and serve as a roadmap for designing small molecules as chemical tools or therapeutic candidates in neurodegenerative disorders.

## Data availability

All experimental details and data supporting the findings of this study are available within the paper and its ESI.† The data are also available from the corresponding authors upon reasonable request.

## Author contributions

M. H. L. and S. P. designed the research. S. P. performed biochemical assays (TEAC assay, cellular ROS assay, AChE assay, dot assay, and gel/western blot), spectroscopic measurements (absorbance and CD), ESI-MS, DFT calculation, and docking studies with data analysis. M. K. carried out TEM measurements, the dot assay, and cell studies. Y. L. and Y.-H. L. collected and analyzed ITC and 2D <sup>1</sup>H-<sup>15</sup>N HMQC NMR data. M. H. contributed to DFT calculation. A. M. and G. N. synthesized **5** and **6**, respectively. J. K. conducted the expression and purification of <sup>15</sup>N-labeled recombinant Aβ<sub>42</sub>. S. P., M. K., M. H., and M. H. L. wrote the manuscript with input from all authors.

## Conflicts of interest

There are no conflicts to declare.

## Acknowledgements

This research is supported by the National Research Foundation of Korea (NRF) grants funded by the Korean government [NRF-2022R1A3B1077319 (M. H. L.); NRF-2022R1A2C1011793 (Y.-H. L.)]; National Research Council of Science & Technology (NST) grant funded by the Korean government [CCL22061-100 (Y.-H. L.)]; KBSI fund (C320000, C330130, and C390000) (Y.-H. L.). M. K. thanks the Sejong Science Fellowship Grants (RS-2023-00214034). J. K. was supported by the National Research,

Development and Innovation Office of Hungary (2018-2.1.17-TÉT-KR-2018-00008) and the Hungarian Academy of Sciences (NAP2022-I-3/2022). We thank Yelim Yi for designing the research and conducting initial experiments and Gunhee Kim for the assistance in TEM studies.

## Notes and references

- 1 P. H. Nguyen, A. Ramamoorthy, B. R. Sahoo, J. Zheng, P. Faller, J. E. Straub, L. Dominguez, J.-E. Shea, N. V. Dokholyan, A. De Simone, B. Ma, R. Nussinov, S. Najafi, S. T. Ngo, A. Loquet, M. Chiricotto, P. Ganguly, J. McCarty, M. S. Li, C. Hall, Y. Wang, Y. Miller, S. Melchionna, B. Habenstein, S. Timr, J. Chen, B. Hnath, B. Strodel, R. Kayed, S. Lesné, G. Wei, F. Sterpone, A. J. Doig and P. Derreumaux, *Chem. Rev.*, 2021, **121**, 2545.
- 2 H. J. Forman and H. Zhang, *Nat. Rev. Drug Discovery*, 2021, **20**, 689.
- 3 M. G. Savelieff, G. Nam, J. Kang, H. J. Lee, M. Lee and M. H. Lim, *Chem. Rev.*, 2019, **119**, 1221.
- 4 I. W. Hamley, *Chem. Rev.*, 2012, **112**, 5147.
- 5 E. Atrián-Blasco, P. Gonzalez, A. Santoro, B. Alies, P. Faller and C. Hureau, *Coord. Chem. Rev.*, 2018, **371**, 38.
- 6 M. P. Mattson, *Nature*, 2004, **430**, 631.
- 7 P. Di Mascio, G. R. Martinez, S. Miyamoto, G. E. Ronsein, M. H. G. Medeiros and J. Cadet, *Chem. Rev.*, 2019, **119**, 2043.
- 8 M. Mital, N. E. Wezynfeld, T. Fraczyk, M. Z. Wiloch, U. E. Wawrzyniak, A. Bonna, C. Tumpach, K. J. Barnham, C. L. Haigh, W. Bal and S. C. Drew, *Angew. Chem., Int. Ed.*, 2015, **54**, 10460.
- 9 J. Han, Z. Du and M. H. Lim, *Acc. Chem. Res.*, 2021, **54**, 3930.
- 10 H. Dvir, I. Silman, M. Harel, T. L. Rosenberry and J. L. Sussman, *Chem.-Biol. Interact.*, 2010, **187**, 10.
- 11 H. Soreq and S. Seidman, *Nat. Rev. Neurosci.*, 2001, **2**, 294.
- 12 Y. Zhang, J. Kua and J. A. McCammon, *J. Am. Chem. Soc.*, 2002, **124**, 10572.
- 13 F. J. Carvajal and N. C. Inestrosa, *Front. Mol. Neurosci.*, 2011, **4**, 19.
- 14 Y. Lin, B. R. Sahoo, D. Ozawa, M. Kinoshita, J. Kang, M. H. Lim, M. Okumura, Y. H. Huh, E. Moon, J. H. Jang, H.-J. Lee, K.-Y. Ryu, S. Ham, H.-S. Won, K.-S. Ryu, T. Sugiki, J. K. Bang, H.-S. Hoe, T. Fujiwara, A. Ramamoorthy and Y.-H. Lee, *ACS Nano*, 2019, **13**, 8766.
- 15 S. J. C. Lee, E. Nam, H. J. Lee, M. G. Savelieff and M. H. Lim, *Chem. Soc. Rev.*, 2017, **46**, 310.
- 16 S. Vivekanandan, J. R. Brender, S. Y. Lee and A. Ramamoorthy, *Biochem. Biophys. Res. Commun.*, 2011, **411**, 312.
- 17 Y. Yi and M. H. Lim, *RSC Chem. Biol.*, 2023, **4**, 121.
- 18 L. M. F. Gomes, J. C. Bataglioli and T. Storr, *Coord. Chem. Rev.*, 2020, **412**, 213255.
- 19 L. Sun, H.-J. Cho, S. Sen, A. S. Arango, T. T. Huynh, Y. Huang, N. Bandara, B. E. Rogers, E. Tajkhorshid and L. M. Mirica, *J. Am. Chem. Soc.*, 2021, **143**, 10462.
- 20 P. Faller, C. Hureau and O. Berthoumieu, *Inorg. Chem.*, 2013, **52**, 12193.



- 21 J. T. Pedersen, J. Østergaard, N. Rozlosnik, B. Gammelgaard and N. H. H. Heegaard, *J. Biol. Chem.*, 2011, **286**, 26952.
- 22 J.-M. Suh, M. Kim, J. Yoo, J. Han, C. Paulina and M. H. Lim, *Coord. Chem. Rev.*, 2023, **478**, 214978.
- 23 S. Park, C. Na, J. Han and M. H. Lim, *Metallomics*, 2023, **15**, mfac102.
- 24 M. Rana, H.-J. Cho, H. Arya, T. K. Bhatt, K. Bhar, S. Bhatt, L. M. Mirica and A. K. Sharma, *Inorg. Chem.*, 2022, **61**, 10294.
- 25 K. P. Kepp, *Chem. Rev.*, 2012, **112**, 5193.
- 26 C. Cheignon, M. Tomas, D. Bonnefont-Rousselot, P. Faller, C. Hureau and F. Collin, *Redox Biol.*, 2018, **14**, 450.
- 27 A. I. Bush, *Trends Neurosci.*, 2003, **26**, 207.
- 28 M. R. Jones, E. Mathieu, C. Dyrager, S. Faissner, Z. Vaillancourt, K. J. Korshavn, M. H. Lim, A. Ramamoorthy, V. Wee Yong, S. Tsutsui, P. K. Stys and T. Storr, *Chem. Sci.*, 2017, **8**, 5636.
- 29 H.-J. Cho, A. K. Sharma, Y. Zhang, M. L. Gross and L. M. Mirica, *ACS Chem. Neurosci.*, 2020, **11**, 1471.
- 30 P. Mecocci and M. C. Polidori, *Biochim. Biophys. Acta, Mol. Basis Dis.*, 2012, **1822**, 631.
- 31 M. Ramesh and T. Govindaraju, *Chem. Sci.*, 2022, **13**, 13657.
- 32 J. W. Arndt, F. Qian, B. A. Smith, C. Quan, K. P. Kilambi, M. W. Bush, T. Walz, R. B. Pepinsky, T. Bussière, S. Hamann, T. O. Cameron and P. H. Weinreb, *Sci. Rep.*, 2018, **8**, 6412.
- 33 J. Seigny, P. Chiao, T. Bussière, P. H. Weinreb, L. Williams, M. Maier, R. Dunstan, S. Salloway, T. Chen, Y. Ling, J. O'Gorman, F. Qian, M. Arastu, M. Li, S. Chollate, M. S. Brennan, O. Quintero-Monzon, R. H. Scannevin, H. M. Arnold, T. Engber, K. Rhodes, J. Ferrero, Y. Hang, A. Mikulskis, J. Grimm, C. Hock, R. M. Nitsch and A. Sandrock, *Nature*, 2016, **537**, 50.
- 34 M. Shi, F. Chu, F. Zhu and J. Zhu, *Front. Aging Neurosci.*, 2022, **14**, 870517.
- 35 K. Servick, *Science*, 2021, **372**, 1141.
- 36 T. Storr, *Can. J. Chem.*, 2021, **99**, 1.
- 37 D. Procházková, I. Boušová and N. Wilhelmová, *Fitoterapia*, 2011, **82**, 513.
- 38 J. L. Baldim, B. G. V. d. Alcântara, O. d. S. Domingos, M. G. Soares, I. S. Caldas, R. D. Novaes, T. B. Oliveira, J. H. G. Lago and D. A. Chagas-Paula, *Oxid. Med. Cell. Longevity*, 2017, **2017**, 3789856.
- 39 N. Mateeva, S. V. K. Eyunni, K. K. Redda, U. Ononuju, T. D. Hansberry, C. Aikens and A. Nag, *Bioorg. Med. Chem. Lett.*, 2017, **27**, 2350.
- 40 T. P. Cushnie and A. J. Lamb, *Int. J. Antimicrob. Agents*, 2005, **26**, 343.
- 41 C. A. Rice-Evans, N. J. Miller and G. Paganga, *Free Radical Biol. Med.*, 1996, **20**, 933.
- 42 S. Sinha, D. H. J. Lopes and G. Bitan, *ACS Chem. Neurosci.*, 2012, **3**, 473.
- 43 A. Tiiman, J. Jarvet, A. Gräslund and V. Vukojević, *Biochemistry*, 2015, **54**, 7203.
- 44 L. N. Zhao, Y. Mu and L. Y. Chew, *Phys. Chem. Chem. Phys.*, 2013, **15**, 14098.
- 45 S. Park, Y. Yi and M. H. Lim, *Bull. Korean Chem. Soc.*, 2021, **42**, 17.
- 46 G. Nam, M. Hong, J. Lee, H. J. Lee, Y. Ji, J. Kang, M.-H. Baik and M. H. Lim, *Chem. Sci.*, 2020, **11**, 10243.
- 47 E. Bendary, R. R. Francis, H. M. G. Ali, M. I. Sarwat and S. El Hady, *Ann. Agric. Sci.*, 2013, **58**, 173.
- 48 H. J. Lee, R. A. Kerr, K. J. Korshavn, J. Lee, J. Kang, A. Ramamoorthy, B. T. Ruotolo and M. H. Lim, *Inorg. Chem. Front.*, 2016, **3**, 381.
- 49 Y. Xie, W. Yang, X. Chen and J. Xiao, *Food Funct.*, 2014, **5**, 2582.
- 50 E. Marzec, M. Świtalska, M. Winiewska-Szajewska, J. Wójcik, J. Wietrzyk, A. M. Maciejewska, J. Poznański and A. Mieczkowski, *IUBMB Life*, 2020, **72**, 1250.
- 51 H. Gao and J. Kawabata, *Bioorg. Med. Chem.*, 2005, **13**, 1661.
- 52 J. S. Derrick, R. A. Kerr, Y. Nam, S. B. Oh, H. J. Lee, K. G. Earnest, N. Suh, K. L. Peck, M. Ozbil, K. J. Korshavn, A. Ramamoorthy, R. Prabhakar, E. J. Merino, J. Shearer, J.-Y. Lee, B. T. Ruotolo and M. H. Lim, *J. Am. Chem. Soc.*, 2015, **137**, 14785.
- 53 M. W. Beck, J. S. Derrick, R. A. Kerr, S. B. Oh, W. J. Cho, S. J. C. Lee, Y. Ji, J. Han, Z. A. Tehrani, N. Suh, S. Kim, S. D. Larsen, K. S. Kim, J.-Y. Lee, B. T. Ruotolo and M. H. Lim, *Nat. Commun.*, 2016, **7**, 13115.
- 54 M. Kim, J. Kang, M. Lee, J. Han, G. Nam, E. Tak, M. S. Kim, H. J. Lee, E. Nam, J. Park, S. J. Oh, J.-Y. Lee, J.-Y. Lee, M.-H. Baik and M. H. Lim, *J. Am. Chem. Soc.*, 2020, **142**, 8183.
- 55 M. Kim and M. H. Lim, *Bull. Korean Chem. Soc.*, 2021, **42**, 1272.
- 56 N. S. Jha, S. Mishra, S. K. Jha and A. Surolia, *Electrochim. Acta*, 2015, **151**, 574.
- 57 M.-H. Baik and R. A. Friesner, *J. Phys. Chem. A*, 2002, **106**, 7407.
- 58 N. J. Jeon, H. G. Lee, Y. C. Kim, J. Seo, J. H. Noh, J. Lee and S. I. Seok, *J. Am. Chem. Soc.*, 2014, **136**, 7837.
- 59 V. J. Forrest, Y. H. Kang, D. E. McClain, D. H. Robinson and N. Ramakrishnan, *Free Radical Biol. Med.*, 1994, **16**, 675.
- 60 P. Pedrielli, G. F. Pedulli and L. H. Skibsted, *J. Agric. Food Chem.*, 2001, **49**, 3034.
- 61 Y. Bourne, J. Grassi, P. E. Bougis and P. Marchot, *J. Biol. Chem.*, 1999, **274**, 30370.
- 62 D. Grisaru, M. Sternfeld, A. Eldor, D. Glick and H. Soreq, *Eur. J. Biochem.*, 1999, **264**, 672.
- 63 N. Andrikopoulos, Y. Li, A. Nandakumar, J. F. Quinn, T. P. Davis, F. Ding, N. Saikia and P. C. Ke, *ACS Appl. Mater. Interfaces*, 2023, **15**, 7777.
- 64 W. Zhang, A. J. Christofferson, Q. A. Besford, J. J. Richardson, J. Guo, Y. Ju, K. Kempe, I. Yarovsky and F. Caruso, *Nanoscale*, 2019, **11**, 1921.
- 65 F. Basagni, M. Naldi, T. Ginex, F. J. Luque, F. Fagiani, C. Lanni, M. Iurlo, M. Marcaccio, A. Minarini, M. Bartolini and M. Rosini, *ACS Med. Chem. Lett.*, 2022, **13**, 1812.
- 66 K. Wähälä and T. A. Hase, *J. Chem. Soc., Perkin Trans. 1*, 1991, 3005.
- 67 Z. Sang, X. Qiang, Y. Li, W. Yuan, Q. Liu, Y. Shi, W. Ang, Y. Luo, Z. Tan and Y. Deng, *Eur. J. Med. Chem.*, 2015, **94**, 348.
- 68 G. Nam, Y. Ji, H. J. Lee, J. Kang, Y. Yi, M. Kim, Y. Lin, Y.-H. Lee and M. H. Lim, *ACS Chem. Neurosci.*, 2019, **10**, 3386.



- 69 M. Sato, K. Murakami, M. Uno, Y. Nakagawa, S. Katayama, K. Akagi, Y. Masuda, K. Takegoshi and K. Irie, *J. Biol. Chem.*, 2013, **288**, 23212.
- 70 J. R. Brender, A. Ghosh, S. A. Kotler, J. Krishnamoorthy, S. Bera, V. Morris, T. B. Sil, K. Garai, B. Reif, A. Bhunia and A. Ramamoorthy, *Chem. Commun.*, 2019, **55**, 4483.
- 71 Y. Xiao, B. Ma, D. McElheny, S. Parthasarathy, F. Long, M. Hoshi, R. Nussinov and Y. Ishii, *Nat. Struct. Mol. Biol.*, 2015, **22**, 499.
- 72 F. Hsu, G. Park and Z. Guo, *ACS Omega*, 2018, **3**, 8401.
- 73 D. Huang, M. I. Zimmerman, P. K. Martin, A. J. Nix, T. L. Rosenberry and A. K. Paravastu, *J. Mol. Biol.*, 2015, **427**, 2319.
- 74 K. J. Korshavn, A. Bhunia, M. H. Lim and A. Ramamoorthy, *Chem. Commun.*, 2016, **52**, 882.
- 75 V. N. Uversky, G. Yamin, P. O. Souillac, J. Goers, C. B. Glaser and A. L. Fink, *FEBS Lett.*, 2002, **517**, 239.
- 76 L. Hou, H. Shao, Y. Zhang, H. Li, N. K. Menon, E. B. Neuhaus, J. M. Brewer, I.-J. L. Byeon, D. G. Ray, M. P. Vitek, T. Iwashita, R. A. Makula, A. B. Przybyla and M. G. Zagorski, *J. Am. Chem. Soc.*, 2004, **126**, 1992.
- 77 A. A. Watson, D. P. Fairlie and D. J. Craik, *Biochemistry*, 1998, **37**, 12700.
- 78 A. M. Brown, J. A. Lemkul, N. Schaum and D. R. Bevan, *Arch. Biochem. Biophys.*, 2014, **545**, 44.
- 79 S.-M. Liao, Q.-S. Du, J.-Z. Meng, Z.-W. Pang and R.-B. Huang, *Chem. Cent. J.*, 2013, **7**, 44.
- 80 J. P. Lee, E. R. Stimson, J. R. Ghilardi, P. W. Mantyh, Y.-A. Lu, A. M. Felix, W. Llanos, A. Behbin, M. Cummings, M. Van Crielinge, W. Timms and J. E. Maggio, *Biochemistry*, 1995, **34**, 5191.
- 81 J.-M. Suh, G. Kim, J. Kang and M. H. Lim, *Inorg. Chem.*, 2019, **58**, 8.
- 82 P. Faller and C. Hureau, *Dalton Trans.*, 2009, 1080.
- 83 C. Cheignon, P. Faller, D. Testemale, C. Hureau and F. Collin, *Metallomics*, 2016, **8**, 1081.

